Biosensors and Bioelectronics: X 32 (2026) 100826

Contents lists available at ScienceDirect

Biosensors and Bioelectronics: X

journal homepage: www.journals.elsevier.com/biosensors-and-bioelectronics-x

Electrolyte-gated organic transistors based on donor-acceptor polymers for DNA biosensing

Kateryna Solodka [a], Alessandro Paradisi [a], Katharina Schmidt [b], Matteo Sensi [a], Marcello Berto [a], Pamela Allison Manco Urbina [a], Roger Hasler [b], Jakub Dostalek [b,c], Wolfgang Knoll [b], Fabio Biscarini [a,d], Marcello Pinti [a], Carlo Augusto Bortolotti [a,*]

[a] Department of Life Sciences, Università di Modena e Reggio Emilia, Via Campi 103, Modena, 41125, Italy
[b] Danube Private University, Steiner Landstraße 124, Krems an der Donau, 3500, Austria
[c] FZU-Institute of Physics, Czech Academy of Sciences, Na Slovance 1999/2, Prague, 182 21, Czech Republic
[d] Center for Translational Neurophysiology of Speech and Communication, Istituto Italiano di Tecnologia, Via Fossato di Mortara 17-19, Ferrara, 44121, Italy

ARTICLE INFO

Keywords:
Electrolyte-gated organic transistor
DNA biosensor
Donor-acceptor polymer
DPP-DTT
Mitochondrial DNA
Label-free detection

ABSTRACT

Electrolyte-gated organic transistors (EGOTs) are emerging as promising devices for biosensing applications due to their high transconductance, ability to operate in liquid environments at low voltages and label-free detection capabilities. In this study, we investigate the performance of EGOTs based on the donor-acceptor polymer DPP-DTT, a material known for its high charge mobility and aqueous stability. The device was tested as a biosensor for the detection of mitochondrial DNA (mtDNA), a biomarker associated with multiple sclerosis, as a model analyte. The gate electrode was functionalized with a complementary DNA probe via surface chemistry, with functionalization efficiency validated by surface plasmon resonance and plasmon-enhanced fluorescence spectroscopy. The resulting DPP-DTT-based EGOT sensor exhibited specific detection of mtDNA in solution, with a detection range from 70 pM to 5 nM. These results highlight the potential of DPP-DTT based EGOTs as stable, sensitive platforms for biosensing applications.

1. Introduction

Electrolyte-gated organic transistors (EGOTs) are promising platforms for biosensing because of their high transconductance, capability of working in a liquid environment at low operational voltage and for label-free detection (Wang et al., 2016). In addition, EGOTs can be interfaced with cells, tissues and living systems for monitoring cell growth (Kyndiah et al., 2025; Spanu et al., 2021; Zhang et al., 2020; Zhao et al., 2023), recording electrophysiological activity (De Salvo et al., 2023), and devising neuromorphic devices (Abouali et al., 2025; Dai et al., 2019). In a typical EGOT, the conductivity of an organic semiconductor channel connecting the source and drain electrodes is modulated by a gate electrode through an electrolyte. Polarization of the gate induces electrical double layers at the gate/electrolyte and semiconductor/electrolyte interfaces, whose high capacitance enables efficient modulation of the channel current (Wang et al., 2016). In biosensing applications, recognition elements can be immobilized either on the semiconductor or on the gate electrode, allowing target binding events at the solid/liquid interface to be converted into measurable changes in the transistor response (Berto et al., 2016; Diacci et al., 2017; Mulla et al., 2015; Solodka et al., 2022; Urbina et al., 2021).

A major limitation of EGOT biosensors is their operational stability in liquid media. Prolonged electrical bias and direct exposure of the semiconductor to aqueous electrolytes may cause drain-source current (I_{DS}) drifts and threshold voltage (V_{th}) shifts. The degradation pathways often involve charge trapping mechanisms, electrochemical reactions at the semiconductor-solution interface and solvent/ion permeation into the OSC layer that can alter its structure and electrical performance, especially in polymeric semiconductors which are more prone to solvent/ion permeability (Bellani et al., 2014; Picca et al., 2019; Segantini et al., 2022; S. Zhang et al., 2023). Hence, in the context of biosensing applications, stabilization protocols are critical to ensure steady output currents, as fluctuations can obscure biosensing signals (Macchia et al., 2018; Molazemhosseini et al., 2021; Picca et al., 2019; Porrazzo et al.,

This article is part of a special issue entitled: Portable biosensors published in Biosensors and Bioelectronics: X.

* Corresponding author.
E-mail address: carloaugusto.bortolotti@unimore.it (C.A. Bortolotti).

https://doi.org/10.1016/j.biosx.2026.100826
Received 18 May 2026; Received in revised form 27 July 2026; Accepted 28 July 2026
Available online 29 July 2026

2014). Additionally, the use of model solution or biological fluids as gating electrolytes such as phosphate buffers, sweat, saliva, blood or serum, can further influence EGOT responses and stability.

Donor-acceptor (D–A) polymers are attractive channel materials for this purpose because their planar conjugated backbones support efficient charge transport (with carrier mobility >1 cm^2 V^{-1} s^{-1}), while their relatively low highest occupied molecular orbital energy (≤ -5.0 eV) can improve stability under aqueous operation (Li et al., 2012). In recent years, interest has grown in *p*-type D–A polymer poly [2,5-(2-octyldodecyl)-3,6-diketopyrrolopyrrole-alt-5,5-(2,5-di (thien-2-yl)thien [3,2-b]thiophene)] (DPP-DTT) (Li et al., 2012). This semiconducting polymer can be easily processed from solutions to obtain thin films or nanowires making it a suitable material for transistor channels (Chennit et al., 2023; Giridharagopal et al., 2021; Y. Zhang et al., 2023). Indeed, DPP-DTT has been exploited for the fabrication of organic field-effect transistors to detect volatile organic compounds (Tran et al., 2023) and interleukin-6 (Y. Zhang et al., 2023), using the device channel as the sensing element. Furthermore, recent studies have reported initial examples where this material was used in the EGOT architecture to fabricate biosensors. These biosensors exploited the gate electrode functionalization to detect various targets in aqueous solutions like 2,4-dichlorophenoxyacetic acid (Nguyen et al., 2018), vascular endothelial growth factor (Pallu et al., 2019) and PFAS (Zanotti et al., 2025). Furthermore, Chennit et al. reported an EGOT fabricated by ink-jet printing of DPP-DTT on a flexible substrate, capable of detecting single-stranded DNA in solution in the micromolar concentration range (Chennit et al., 2023). Despite these advances, the systematic assessment of DPP-DTT-based EGOT stability during repeated operation in aqueous electrolytes, together with label-free detection of single-stranded DNA at sub-nanomolar concentrations, has not yet been extensively investigated.

In this work, we evaluated the stability in different aqueous electrolytes of a DPP-DTT-based EGOT, together with its biosensing capabilities for detecting DNA single strands in solution, focusing on a sequence specific to mitochondrial DNA (mtDNA). Elevated circulating mtDNA levels in cerebrospinal fluid and plasma have recently been observed in multiple sclerosis (MS) patients (Nasi et al., 2020; Varhaug et al., 2017). Since identifying reliable biomarkers for MS remains a critical challenge, developing biosensors targeting mtDNA could support the development of diagnostic or monitoring tools. To achieve sensitivity to the specific mtDNA sequence, we functionalized the gate electrode of the EGOT device with a complementary single stranded DNA through surface chemistry. The functionalization efficiency and the ability to specifically bind the target single-stranded DNA in solution were validated using surface plasmon resonance (SPR) and surface plasmon-enhanced fluorescence spectroscopy (SPFS). After stabilization, the DPP-DTT-based EGOT sensor demonstrated specific detection of mtDNA sequences across a concentration range of 70 pM to 5 nM.

2. Materials and methods

2.1. Materials

All the reagents and materials were used as provided from the manufacturer without further purifications. The DPP-DTT was purchased from Ossila Ltd. (MW = 111 kDa). The OEG (11-mercaptoundecyl-triethylene glycol) was purchased from Sigma-Aldrich (Merck Life Science, Milano, Italy) and biotin-OEG (TH 004-m11.n6) was purchased from Prochimia Surfaces (Advanced Wave Sensors, Paterna, Spain); neutravidin was obtained from Thermo Fisher Scientific; while the DNA single strands (Table 1) were purchased from Integrated DNA Technologies. The target mtDNA sequence was selected by using the online informatics tool Primer3plus and tested with Primer Blast from NCBI.

Table 1
Oligonucleotide sequences used in this study.[a].

Capturing sequence (P-DNA)	5′-Biotin-AAA AAA TTA CCG GGC TCT GCC ATC T-3′
Complementary sequence (C-DNA)	3′-AAT GGC CCG AGA CGG TAG A-5′
Fluorescently labelled complementary sequence (LC-DNA)	3′-AAT GGC CCG AGA CGG TAG AAA AAA A–AlexaFluor647-5′
Non-complementary sequence (NC-DNA)	5′-TAA CAA CAT ACC CAT GGC CA-3′

[a] The red-labelled nucleotides indicate the target mtDNA sequence and its complementary sequence, used in this study.

2.2. Device fabrication

The EGOT transistors were fabricated using gold interdigitated source and drain electrodes patterned on glass substrates. These electrodes were purchased from MicruX Technologies (Asturias, Spain). The electrodes presented a $L = 10$ μm and a $W = 490$ mm (W/L = 49000) and were made of Au deposited on top of a Ti adhesive layer of 150 and 50 nm thickness, respectively. Before the semiconductor deposition, the substrates were cleaned by sonication in a 1% *v/v* Hellmanex™ III aqueous solution, followed by sonication in H_2O, and finally sonication in ethanol. Every sonication step lasted for 15 min. Once the cleaned procedure was completed, the substrates were dried gently under N_2 flow. A solution of the polymer DPP-DTT (5 mg mL^{-1} in 1,2-dichlorobenzene) was deposited on top of the substrates by spin coating. After DPP-DTT deposition, the substrates were cured in the oven at 140 °C for 45 min. Finally, the devices were stored in a 50 mM Na-phosphate buffer at pH 7.4 until they were used in the experiments.

2.3. Electrical characterization

All the electrical measurements were performed at room temperature inside a Faraday cage. Source, drain, and gate electrodes were connected to an Agilent B2902A Source Measure Unit, and the electrical redout was acquired by means of a personalized control software. An Au wire (Au 99.99%, 1 mm Ø, 1 mm^2 area), immersed in the electrolyte, was used as the gate electrode during the experiments. Transfer characteristics were acquired by sweeping gate-source potential (V_{GS}) between −0.7 V and 0 V, at a constant $V_{DS} = -0.1$ V, in the electrolyte, confined inside a PDMS pool. Before performing the characterization and sensing experiments, the EGOT devices were stabilized by recording consecutive transfer curves until I_{DS} stability. Then the electrolyte solution was replaced with a fresh one from the stock solution and the consecutive recording was repeated until no further significant changes in I_{DS} could be measured.

The mtDNA sensing measurement with the EGOT devices used a functionalized gate electrode, prepared as reported below. The mtDNA sensing data are reported as average values from five independent measurements/devices, and error bars represent the standard error of the mean. The LOD threshold was calculated from the non-specific binding control as $S_{LOD} = S_0 + 3\sigma$, where S_0 is the average signal from three measurements and σ is the corresponding standard deviation.

2.4. Gate functionalization

The Au wires were cleaned according to the following procedure: *i*) immersion in 2.5 M KOH at 130 °C for 4 h, *ii*) immersion in 96% *v/v* H_2SO_4 at 220 °C for 2 h, *iii*) rinsing with water. The Au wires were functionalized as follows: *i*) overnight incubation in a mixture of SAM forming molecules: biotin-OEG 0.1 mM, OEG 0.9 mM in ethanol, *ii*) rinse with ethanol, *iii*) incubation with 2 μM NeutrAvidin in PBS with 0.05% *w/v* Tween-20 pH 7.4 solution (PBS-T) for 30 min, i*v*) rinse with PBS-T, *v*) incubation with a 200 nM P-DNA in PBS-T for 20 min, *vi*) rinse with PBS-T, and *vii*) incubation in PBS-T, prior to the electrical measurements. All the functionalization steps were performed at room

temperature. The area of the gate electrode was kept constant by means of a passivation layer.

2.5. SPR-SPFS

The gate electrode functionalization procedure was characterized optically with SPR and SPFS in the Kretschmann configuration (Kretschmann and Raether, 1968). The sensor chips were prepared by evaporating Au, with a thickness of 50 nm, on BK7 glass slides, with a Cr adhesive layer of 2 nm. Then, the Au slides were rinsed with ethanol and H_2O, dried, and cleaned with UV-ozone for 20 min. Cleaned Au slides were immersed overnight in a SAM forming solution of biotin-OEG and OEG (0.1 mM and 0.9 mM in ethanol, respectively). The SAM-functionalized Au slides were rinsed with ethanol to remove the excess of SAM, and gently dried with N_2 flow. The optical configuration based on total internal reflection used a beam emitted from a HeNe laser passed through a laser band-pass filter, a polarizer, and a neutral density filter (1%). A TM polarized beam at the wavelength $\lambda_{ex} = 633$ nm with the intensity of 1.5 μW was coupled to a 90° prism coupler made of LASFN9 glass. The Au slide was optically matched to the prism base using immersion oil. In order to delimit the liquid sample, a flow cell was clamped on the surface of the sensor chip. The flow cell, with a volume of 10 μL, was made from a thin PDMS gasket and sealed by a transparent fused silica glass substrate. Inlet and outlet ports were drilled into the silica substrate, that were connected by tubing to a peristaltic pump. The angle of incidence θ of the excitation beam hitting the gold sensor surface was adjusted at the reflectivity minimum in order to assure the resonant coupling to SPs at the interface with an aqueous sample. The enhanced field intensity of SPs excited randomly oriented fluorophore labels at the distance from the gold sensor surface. The emitted fluorescence light at $\lambda_{em} = 670$ nm was collected by a module with a lens and passed through a set of filters consisting of a notch filter that was used to block the excitation wavelength λ_{ex} and two bandpass filters with the transmission window centred at the $\lambda = 670$ nm and spectral width of about 10 nm. The fluorescence beam was focused on the input of a photomultiplier (H6240-01, Hamamatsu, Japan) that was connected to a counter (53131A from Agilent, USA). The output from the counter was recorded in counts per second (cps) by using software Wasplas developed at the Max Planck Institute for Polymer Research in Mainz (Germany). The detailed description of the SPFS setup is described in reference in Hageneder S. et al. (Hageneder et al., 2016)

During the assay, the binding of the neutravidin molecules to the exposed biotin moieties of the SAM surface and the further immobilization of the capturing P-DNA probes was monitored by SPR. A solution of PBS-T was flushed into system (30 μL min^{-1}), which served as the baseline, and the SPR signal was recorded by measuring the reflected beam intensity. Then, the Au slide was incubated with a neutravidin solution (2 μM in PBS-T) for 30 min, and with a solution containing the capturing P-DNA, 200 nM in PBS-T, for 20 min (Fig. S1). Following the immobilization of P-DNA on the Au surface, samples containing increasing concentrations of labelled complementary LC-DNA, ranging from 0.5 nM to 100 nM, was continuously flushed into the system. Following every incubation step, a washing step was done by flushing PBS-T into the system for 10 min.

Please note that, during the SPFS experiments, all solutions were prepared in a buffer solution containing PBS buffer with 0.05% v/v Tween 20, while during the electrical experiments, in order to avoid the contact of the detergent agent with the organic semiconductor, the measurements were performed using only PBS. Nonetheless, prior to the electrical measurements, a final functionalization step, consisting of incubation in PBS buffer with 0.05% *v/v* Tween 20 (for 15 min), was included with the aim of reducing non-specific binding.

The angular reflectivity scans were fitted with a Fresnel reflectivity-based model, using the Winspall 3.02 software, in order to determine the thickness of the biolayers on the gold surface. The fitting allowed the determination of the thickness and the apparent refractive index values for the employed SPR glass slide. These values were further employed as reference for the simulation of thickness changes induced by the biolayer formation. The surface mass density Γ (ng mm^{-2}) was determined by applying Feijter's equation (Homola, 2008; Homola et al., 1999):

$$\Gamma = d_p(n_p - n_s)\left(\frac{\partial n}{\partial C}\right)^{-1}$$

Where d_p is the thickness of the biolayer, n_p is the refractive index of the biolayer, n_s is the refractive index of the aqueous solution in contact with the biolayer, and dn/dC is the refractive index increment of the adsorbed biolayer, which is typically set to 0.2 mm^3 mg^{-1} for biolayers (Hasler et al., 2022; Perlmann and Longsworth, 1948). The determination of Γ for each biolayer allowed to estimate the grafting density σ (nmol mm^{-2}) of immobilized protein and P-DNA molecules, with the relation $\sigma = \Gamma/MW$. The obtained data are reported in Table S1.

The binding curves of the LC-DNA samples with P-DNA recorded with the SPFS setup were fitted with exponentials functions, assuming a Langmuir binding model, to obtain the values of the fluorescence plateau (equilibrium values) for each sample concentration. Then, fluorescence changes (ΔF) for each sample were obtained by subtracting the baseline fluorescence signal (absence of analyte) from the plateau value. The associated errors at each concentration were estimated form the standard errors of the fit.

3. Results and discussion

3.1. EGOT characterization

In the context of EGOT-based biosensors, a stable response of the device is fundamental to correctly distinguish between the specific signal variations ascribed to analyte sensing parasitic fluctuations of the device current due to other effects. Generally, the sensor response is defined in terms of relative variation of one (or more) characteristic electrical parameters (such as the channel current I_{DS}, the transconductance g_m, and threshold voltage V_{th}) as a function of the analyte concentration. However, device instability generally manifests itself in the form of drift/fluctuations of such parameters over time. In addition, the magnitude of these variations can also be influenced by the chemical nature of the electrolytes in solution, with a possible influence on the device sensing capabilities. Hence, a stabilization protocol performed before the actual sensing experiment is fundamental to ensure reliability of the measurements (Macchia et al., 2018; Molazemhosseini et al., 2021; Picca et al., 2019).

For these reasons, the fabricated DPP-DTT devices were first evaluated in terms of variations of I_{DS}, g_m, V_{th}, and stability in aqueous solutions that mimics biological fluids: phosphate buffered saline (PBS), artificial sweat (ASw), artificial saliva (ASal) and artificial wound exudate (AWE). The composition of the electrolyte solutions used in this study are reported in Table S1, while the details of the fabrication procedure are reported in the **Materials and methods** section. To characterize the electrical properties of the device, transfer curves were recorded by scanning the gate potential (V_{GS}) between 0 V and −0.7 V, at constant $V_{DS} = -0.1$ V. A bare gold wire was used as a gate electrode (Fig. 1a). As a stabilization procedure, consecutive transfer curves were recorded until superimposable curves were obtained. At this point the electrolyte solution was replaced with a fresh one and the consecutive acquisition of transfer curves was repeated. This protocol was followed until no clear drift of the recorded current could be detected. The device stability was defined as % standard deviation of the average transfer curve current (I_{DS}) obtained from the last three electrolyte change steps. The fluctuations of the device transfer curve (or of the related electrical parameters) in the absence of the analyte (*i.e.* a blank sample) are often chosen to define the standard deviation of the blank sample in the calculation of the theoretical limit of detection (LOD) of the sensor; hence, it is an important figure of merit of the sensor performance.

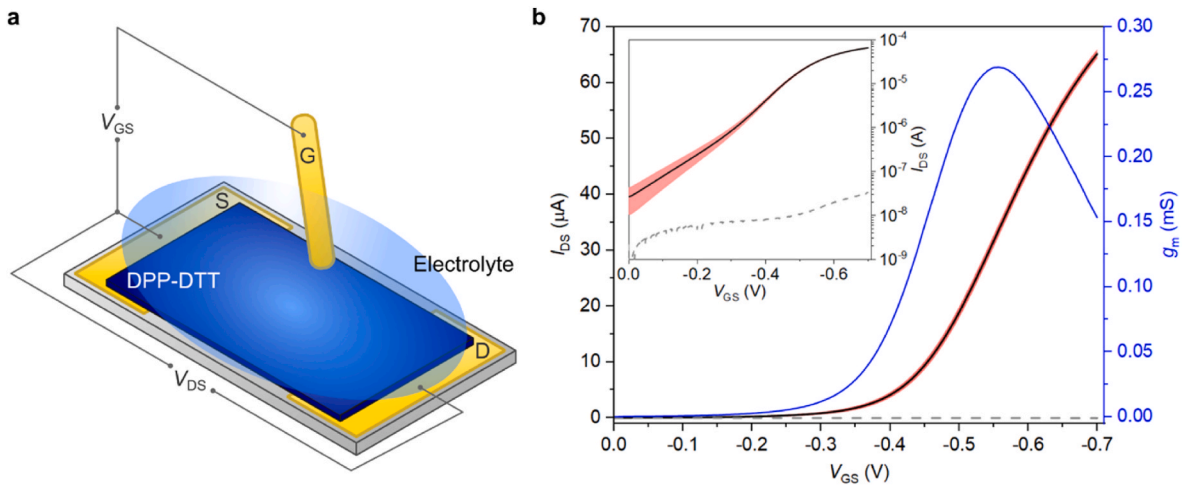

Fig. 1. (a) Schematic representation of the EGOT device configuration. The organic semiconductor layer (OSC) corresponds to the DPP-DTT layer, while the S, D and G labels indicate the source, drain and gate electrodes, respectively. (b) Average transfer curve (black trace) of three different electrolyte samples of PBS buffer after the stabilization procedure, together with the associated standard deviation ($n = 3$, red shaded area). Transconductance curve (blue trace, right axis) associated with the average transfer curve and respective leakage current (I_{GS}, dashed grey trace). The transfer curves were recorded at $V_{DS} = -0.1$ V using a bare gold electrode as gate. Inset: transfer and leakage currents curves on a Log-lin scale. (For interpretation of the references to colour in this figure legend, the reader is referred to the Web version of this article.)

Using PBS as gating electrolyte, the DPP-DTT based EGOT devices are characterized by a threshold voltage $V_{th} = (-464 \pm 5)$ mV and reach a maximum I_{DS} of ~65 μA at $V_{GS} = -0.7$ V; the maximum $g_{m(max)} = (0.25 \pm 0.04)$ mS is recorded at $V_{GS} \sim -0.55$ V (Fig. 1b and Table S2). In terms of stability, the average transfer curve I_{DS} has a 1.1% relative standard deviation, calculated over the measurements of three electrolyte blank samples. This result suggests a good short-term stability of our devices and it is consistent with a report by Zhang et al. on long-term stability of a DPP-DTT based EGOT (Zhang et al., 2020).

On the other hand, the effect of the other electrolytes as gating solutions on these parameters is significant: the threshold voltage V_{th} varies in a range of about 150 mV, from ~ −530 mV in AWE to ~ −410 mV in Asal (Table S2). Similarly, the maximum transconductance $g_{m(max)}$ varies from a minimum of 120 μS (in AWE) to a maximum of 250 μS (in PBS). The electrolyte solutions also have a significant effect on the stability of the EGOT device (Table S3): the relative standard deviation of I_{DS} recorded in PBS is ~1%, whilst the ones extracted in ASw and AWE are about four times larger (~4%). Based on these data alone, it is not possible to investigate the molecular determinants of these differences and more specific studies will be necessary. However, recently it was demonstrated that the transport properties of mixed ionic/electronic conductors depends on the chemical nature of the ions used as electrolytes (Cendra et al., 2019; Coutinho et al., 2023; Flagg et al., 2018; Wu et al., 2021). In particular, for polymeric *p*-type semiconductors that work in accumulation mode (like DPP-DTT), properties such as hole mobility, g_m and V_{th} of the device depend on the type of anions present in solution: the OSC is doped with different efficiency by different anions, depending on their size and solvation spheres (Cendra et al., 2019; Coutinho et al., 2023; Flagg et al., 2018; Wu et al., 2021). Hence, it is likely that the differences in anions composition between the electrolyte solutions tested in this work are responsible for the variations in the electric properties of DPP-DTT-based EGOTs.

Overall, these data show that the composition of the electrolyte affects the electrical characteristics of the DPP-DTT-based EGOT, but do not prevent its use in these different media. In fact, in all considered cases, the transistors maintain excellent electrical properties and good stability. Nonetheless, these chemical effects should be kept in consideration during the design of a (bio)sensor, as they can affect the performance and the sensitivity of the device.

3.2. Gate electrode functionalization for mitochondrial DNA sensing

The DPP-DTT-based EGOT exhibited excellent electric performances in various aqueous electrolytes, motivating us to explore its potential as a biosensor for detecting specific DNA single strands sequences in buffered solutions. In several biosensing applications, the gate functionalization proved a very robust and versatile strategy to decorate the electrode surface with a rich variety of molecules (Aspermair et al., 2020; Diacci et al., 2017; Mulla et al., 2015; Sensi et al., 2023; Thomas et al., 2018; Urbina et al., 2024; Zanotti et al., 2025). To confer sensitivity to the target mtDNA sequence, we functionalized the gold gate electrode with a complementary single stranded DNA sequence serving as a capturing probe (P-DNA) at the gate/electrolyte interface. The target mtDNA sequence was selected because it is specific to mtDNA and does not cross-react with pseudo-mitochondrial sequences in nuclear DNA. Furthermore, it is in a conserved region of the mtDNA, not commonly targeted by specific mutation or disease-associated variant, making it an excellent target for circulating mtDNA detection.

The P-DNA consists of a single-stranded sequence composed by 19 nucleotides, with an additional 6 adenine nucleotides serving as spacer, and a biotin molecule tag at the 5' end. The biotin-tag enabled the immobilization of P-DNA on the gold surface using a biotinylated self-assembled monolayer (SAM) combined with a layer of neutravidin (Fig. 2a). The neutravidin-biotin (or streptavidin-biotin) complex is characterized by an exceptionally strong non-covalent interaction, making it highly effective for such applications. The reported affinity constant of $K_a = 2.5 \times 10^{13}$ between streptavidin and biotin, together with the fact that biotin can be linked to almost any biomolecule, make the exploitation of this complex a workhorse in biotechnology (Dundas et al., 2013). To form the biotinylated SAM on the gold surface, we used a mixture of oligo-ethyleneglycol-alkanethiol (OEG) and biotinylated-OEG. With respect to the commonly used biotinylated-alkanethiols, OEG layers are widely employed to prevent fouling at the electrode surface while maintaining hydrophilicity and reducing the decay of the Debye-length in buffer solutions with high ionic strength. This property enhances the sensitivity of the device, enabling the detection of binding events at distances longer than 1–2 nm, which is the typical Debye-length for a metal electrode in physiological buffer solutions (Gao et al., 2015; Haustein et al., 2019).

We performed a detailed characterization of the functionalization process by SPR. This is a standard technique that allows to measure

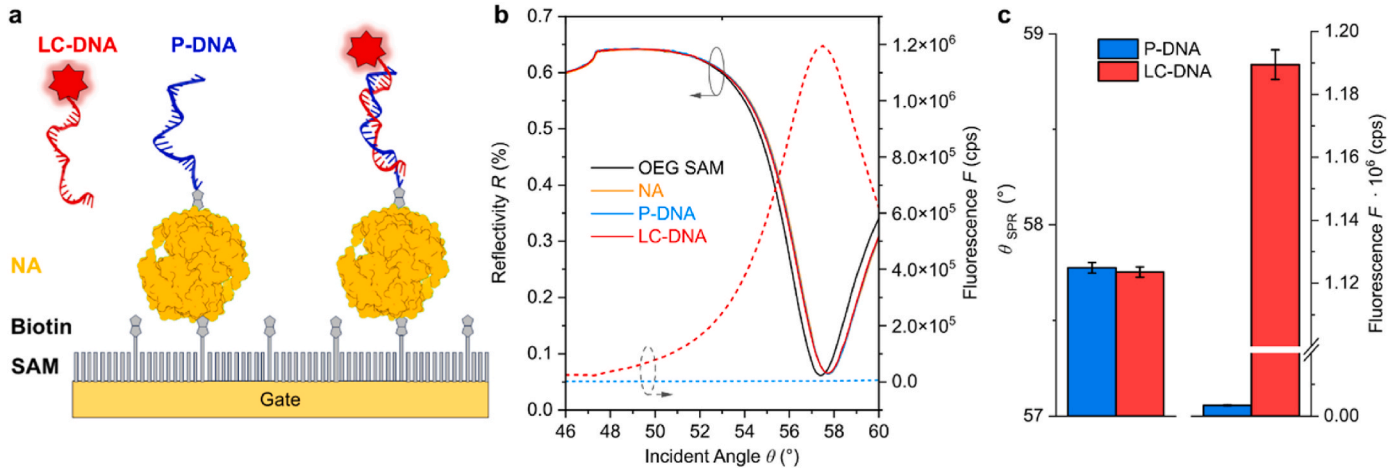

Fig. 2. (a) Cartoon representation of the gate functionalization process used for SPR-SPFS measurements and the binding assays for the C-DNA in solution. (b) Angular reflectivity scans (solid lines, left axis) recorded for the different functionalization steps and corresponding fluorescence intensity curve (dashed lines, right axis), following the hybridization of 1 nM C-DNA on the gold surface. (c) Angle of minimum reflectivity (left axis) for the gold surface functionalized with P-DNA and with bound LC-DNA (10 nM). Fluorescence intensity signal for the gold surface the surface functionalized with P-DNA and with bound LC-DNA (10 nM). Data are reported as average values with the associated standard deviation ($n = 3$). (For interpretation of the references to colour in this figure legend, the reader is referred to the Web version of this article.)

biomolecular interactions happening at functionalized surfaces, their dependence on experimental conditions and the reproducibility of the functionalization procedure (Bhalla, 2026; Hojjat Jodaylami et al., 2025). Here, the angular reflectivity scans recorded at the different steps of the functionalization procedure, reported in Fig. 2b allowed the measurement of the biolayers thickness and of the associated surface mass density (Γ). These parameters were obtained by fitting the angular reflectivity scans to a model based on Fresnel's theory and the results are reported in Table S4. The P-DNA has a $\Gamma = 20$ ng cm^{-2} which is equivalent to 1.5×10^{12} molecules cm^{-2} (P-DNA MW = 8 kDa), *i.e.* binding sites for the target DNA sequence. These values are in line with those previously reported in the literature for this immobilization strategy (Blasi et al., 2020; Su et al., 2005). In addition, from the calculated molecular densities (Table S4), a binding ratio of ~0.68 between biotinylated P-DNA and neutravidin is obtained. Assuming that after the neutravidin binding to the biotin moieties of the SAM, two biotin-binding sites per protein molecule remain accessible, a maximum theoretical ratio of 2 would be expected; however, the distance between the two biotin-binding sites is close to the hydrodynamic diameter of DNA, which results in electrostatic repulsion and, together with steric hindrance, prevents the efficient binding of two biotinylated DNA strands per one single molecules of neutravidin (Hasler et al., 2022; Kotlarek et al., 2020).

In order to confirm the effective binding of the target DNA sequence to the functionalized surface, we characterized the DNA hybridization reaction (Fig. 2a) between P-DNA on the gold surface and its complementary sequence, at different concentrations. However, due to the small molecular size of the target DNA sequence, the hybridization reaction could not be effectively monitored using SPR, as no significant shifts in the refractive index of the system were detected, as shown in Fig. 2b (solid lines) and Fig. 2c. To address this limitation, we employed an assay based on SPFS. In this assay, we employed a labelled version of the complementary DNA strand target (LC-DNA): the strand featured the complementary sequence to the P-DNA, together with an additional short sequence of six adenine nucleotides serving as a spacer for the conjugation with a fluorescent label at the 3' end (LC-DNA, 25 nucleotides), as shown in Fig. 2a (Hageneder et al., 2016; Toma and Tawa, 2016).

The SPFS technique takes advantage of the amplification of the fluorescence intensity emitted by a chromophore employed as a label. The emitted fluorescence intensity can be increased by the coupling with the confined surface plasmon-enhanced field intensity at the emitter absorption wavelength (leading to locally increased excitation rate) and improved quantum yield (due to the increased local density of optical states) at the emission wavelength (Liebermann and Knoll, 2000; Mor et al., 2025). The intensity of the optical field at the metal/solution interface is enhanced with respect to the incoming laser light in the used SPR setup, in which there was used a transparent flow-cell and a unit for collecting and detection of fluorescence light emitted in the perpendicular direction. As seen Fig. 2b (red dashed trace), the fluorescence intensity can be measured as function of angle of incidence of the excitation laser beam θ and the plasmonic enhancement is manifested as a peak at the angle, where SPR occurs and thus the reflectivity drops (Hageneder et al., 2016; Liebermann and Knoll, 2000; Mor et al., 2025).

The blue trace in Fig. 3a shows the gradual increase in fluorescence intensity (measured at in time at the angle fix close to that where the maximum enhancement occurs) following the injection of the LC-DNA samples at increasing concentrations. This increase is associated to the specific binding of LC-DNA to P-DNA on the functionalized gold surface. Each injection step is followed by a short washing step of 10 min, to remove the LC-DNA remained in the bulk of the solution. This washing step is associated with a slow reduction in fluorescence due to the dissociation reaction. The binding kinetics of LC-DNA to P-DNA exhibits exponential trend and saturates at equilibrium values ($\Delta F = F - F_{\text{baseline}}$). However, for low analyte concentrations (C < nM) the kinetics appears to be a relatively slow process happening over the hours timescale. Therefore, we extrapolated the equilibrium fluorescence values at each LC-DNA concentration ΔF, by fitting the kinetics traces $F(t)$ with a Langmuir binding model, as shown in Fig. 3a (dashed traces). The extrapolated equilibrium values were plotted as a function of the [LC-DNA] as shown in Fig. 3b. ΔF shows a clear dependence on the concentration of the target analyte, following a monotonic increasing trend with respect to [LC-DNA]. To estimate an association binding constant for the LC-DNA/P-DNA pair, the ΔF *vs* [LC-DNA] data were fitted with a Langmuir isotherm model using the following equation:

$$\Delta F = \Delta F_{\max} \frac{K_a\,[\text{LC}-\text{DNA}]}{1 + K_a[\text{LC}-\text{DNA}]}$$

The fitting of the experimental data gives an association binding constant of $K_a = (3.5 \pm 1.8) \times 10^8$. Overall, the SPFS characterization demonstrated that the target DNA sequence can efficiently bind at the sensor functionalized surface.

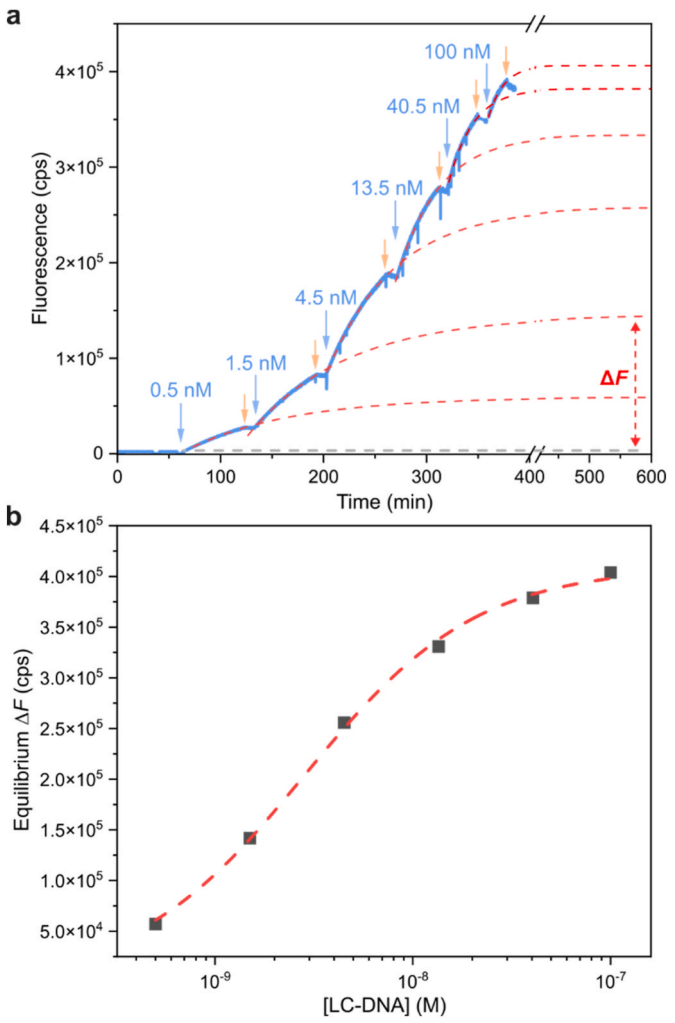

Fig. 3. (a) Fluorescence intensity *vs* time (blue trace), following the injection of samples with increasing concentration of labelled LC-DNA concentrations (blue arrows). Orange arrows indicate the washing step, with an injection of PBS-T buffer. The red dashed traces represent the fittings of the binding kinetics with a Langmuir binding model. The dashed double arrow shows how the ΔF values were obtained for each LC-DNA concentration. They grey dashed line shows the baseline fluorescence signal in the absence of LC-DNA. (b) Equilibrium fluorescence variation at different labelled LC-DNA concentrations. These values were obtained from fitting of the binding kinetics. The red dashed line represent the Langmuir isotherm fit (red dashed line). The associated standard deviations for each data point are <5% of the relative ΔF value and hence smaller that the size of the data marker. (For interpretation of the references to colour in this figure legend, the reader is referred to the Web version of this article.)

3.3. DNA sensing with EGOT

The functionalized gold surface was then employed as a gate electrode in the EGOT device to perform biosensing experiments. Here, it was exposed to sample solutions of C-DNA in PBS buffer, pH 7.4, which were also acting as the gating electrolyte for the transistor. The C-DNA concentration range tested was from 1 pM to 10 nM. For each sample, we measured the transfer characteristic of the device until stabilization, which is reached in about 15–20 min. Following the exposure to C-DNA, the measured I_{DS} increases as a function of the C-DNA concentration (Fig. 4a). The sensor signal (S) was quantified as relative I_{DS} change with respect to the blank sample (without C-DNA): $S = \Delta I_{DS}/I_{DS,0}$; where ΔI_{DS} is the difference between the I_{DS} measured at a certain C-DNA concentration minus the current measured without the target analyte $I_{DS,0}$ at $V_{GS} = -0.6$ V. As shown in Fig. 4b, the measured signal shows low sensitivity for C-DNA in the 1–50 pM concentration range, then rapidly increases monotonically until a plateau value (S ~0.75–0.80) at [C-DNA] $\geq$ 5 nM.

Control experiments were conducted to assess the selectivity of the biosensor response to the target DNA sequence. The response was tested using a non-complementary DNA sequence (NC-DNA) to assess potential non-specific interactions with the functionalized gate surface and/or the semiconductor channel. This NC-DNA, which shares a 35% sequence similarity with the C-DNA sequence, was tested at a concentration of 5 nM and 10 nM. Both these samples produced a very similar low response (Fig. 4c). Furthermore, in a second set of control experiments, the non-specific binding of C-DNA to the surface was evaluated in the absence of P-DNA anchored on the electrode surface. Together, these controls revealed a small signal attributable to non-specific interactions (Fig. 4c), which could interfere with accurate detection of C-DNA at very low concentrations. To quantify this limitation, the signal corresponding to the biosensor's limit of detection (S_{LOD}) was calculated based on the control experiment using a gate surface without P-DNA functionalization, where only non-specific interactions occurred. The S_{LOD} was calculated as $S_{LOD} = S_0 \pm 3\sigma$, where S_0 is the average measured signal ($n = 3$) and σ is the associated standard deviation. The resulting $S_{LOD} = 0.27$ indicates that signals measured in the 1–50 pM concentration range are unreliable and likely influenced by non-specific binding interactions. Indeed, the sensitivity to the target analyte in this concentration range is very low, as the device was unable to distinguish between the 1 pM and the 50 pM standard samples.

Furthermore, the dose-response curve of the biosensor was then fitted with a Langmuir isotherm, to extract a quantitative relationship between the signal S and the [C-DNA]:

$$S = S_{max}\frac{K_a\,[\mathrm{C-DNA}]}{1 + K_a[\mathrm{C-DNA}]}$$

where S_{max} is the maximum value reached at the plateau and K_a is the equilibrium association constant of the binding between P-DNA and C-DNA. The data point at 1 pM was excluded from the fitting procedure as the corresponding signal is below the S_{LOD}. From the best fit curve (Fig. 4b, red dashed line), we determined $K_a = (6 \pm 1) \times 10^9$ at $V_{GS} = -0.6$ V. On the basis of this curve, the concentration corresponding to S_{LOD} is equal to 70 pM. The apparent association constant derived from the EGOT response is approximately one order of magnitude higher than that obtained from the SPFS measurements. The available data do not allow to establish the origin of this discrepancy, but several factors may contribute. First, the fluorescently labelled DNA construct used in the SPFS experiments contains both an additional spacer sequence and a fluorophore, which may influence its hybridization with the surface-immobilized P-DNA. One possibility is that the presence of the fluorescent tag sequence, required for the SPFS experiment, could reduce the binding affinity with the P-DNA strands on the surface. An alternative possibility is that the presence of an electric field at the gate/electrolyte interface, induced by the applied V_{GS}, could also influence the binding affinity of the C-DNA/P-DNA, as previously reported for EGOT based systems (Berto et al., 2016; Urbina et al., 2021).

In terms of sensing mechanism, two of the major contributions that play a role in EGOT sensing are the change of the effective capacitance of the device and/or the shift of the device threshold voltage (V_{th}) (Picca et al., 2020; Torricelli et al., 2021). The analysis of the transfer curves from the sensing experiments shows the increase in current recorded upon C-DNA binding is accompanied by a very small change in V_{th} (ΔV_{th} < 5 mV, with respect to the blank samples), while a significant change in transconductance g_m occurs, as shown in Fig. 4d. The transconductance depends on both the effective device capacitance and the charge-carrier mobility of the semiconductor; however, since molecular recognition occurs at the gate/electrolyte interface rather than directly at the semiconductor channel, it is reasonable to hypothesize that the observed

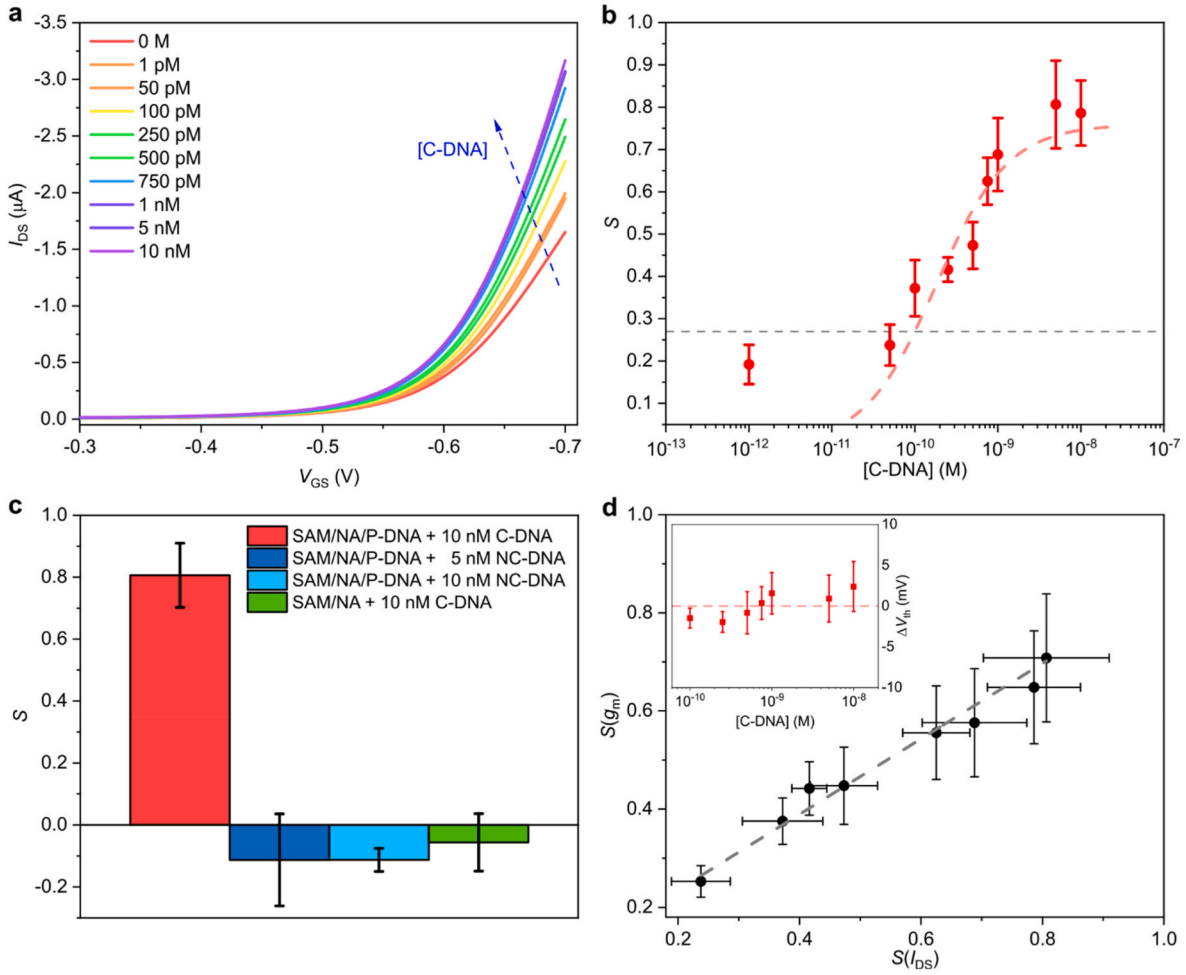

Fig. 4. (a) Representative transfer curves measured at increasing concentration of C-DNA in PBS solution, at $V_{DS} = -0.1$ V. (b) Dose-response curve *S vs* [C-DNA], with *S* measured at $V_{GS} = -0.6$ V; the dashed red line is a Langmuir isotherm fitting of the experimental points; the grey dashed line indicates the signal corresponding to the theoretical LOD. (c) Comparison of the signal obtained with the EGOT biosensor at $V_{GS} = -0.6$ V obtained by exposing the device to 10 nM C-DNA (red), 5 nM NC-DNA (blue) and 10 nM NC-DNA (light blue); the green bar represents the signal obtained by exposing the gate without P-DNA on the surface to 10 nM C-DNA. (d) Correlation plot of the signal obtained from I_{DS} change (S_{IDS}) *vs* the signal obtained from g_m change (Sg_m), at each C-DNA concentration, calculated at $V_{GS} = -0.6$ V, with associated standard errors. The slope of the linear fit (dashed line) is 0.80. Inset: variation of V_{th} with respect to the blank sample as function of [C-DNA]; the red dashed line represents the $\Delta V_{th} = 0$ mV reference. All data points are reported as average values ($n = 5$) with the corresponding experimental errors are reported as standard error. (For interpretation of the references to colour in this figure legend, the reader is referred to the Web version of this article.)

response is consistent with a predominantly capacitive contribution.

4. Conclusions

The donor-acceptor polymer DPP-DTT is an excellent material to fabricate a EGOT devices for biosensing applications. We showed that a conditioning procedure for the device performed prior to the sensing measurements is a key step to ensure the device stability in terms of electrical parameters in various biologically relevant solutions. To demonstrate the device sensing capabilities, we employed it as a biosensor for DNA single strand detection in solution and used a particular sequence of mtDNA as molecular target. SPR and SPFS have been used to validate the sensing strategy through optical monitoring of the functionalization steps of the gold electrode and the affinity interaction with target analyte. The SPFS- and EGOT-based sensors relied on identical biointerfaces and the measured calibration curves showed similar character with comparable K_a constant, with deviations that can be attributed to the effect of the readout mechanism (*e.g.* errors in SPFS data due to the fluorescence bleaching and potential changes in the affinity interaction characteristics due to the applied potential at the used gold electrode for EGOT). Conversely, the EGOT-based sensor can detect increasing concentration of complementary mtDNA sequences in the 70 pM to 5 nM range. The sensing assay results demonstrated that the DPP-DTT is an excellent organic semiconductor to fabricate robust and high-performing EGOT biosensors.

CRediT authorship contribution statement

Kateryna Solodka: Data curation, Formal analysis, Investigation, Methodology, Writing – original draft, Writing – review & editing. **Alessandro Paradisi:** Formal analysis, Methodology, Validation, Visualization, Writing – original draft, Writing – review & editing. **Katharina Schmidt:** Investigation, Methodology, Validation, Writing – review & editing. **Matteo Sensi:** Conceptualization, Methodology, Validation, Visualization, Writing – review & editing. **Marcello Berto:** Formal analysis, Investigation, Validation, Writing – review & editing. **Pamela Allison Manco Urbina:** Investigation, Methodology, Validation, Writing – review & editing. **Roger Hasler:** Data curation, Formal analysis, Methodology, Validation, Writing – review & editing. **Jakub Dostalek:** Formal analysis, Resources, Supervision, Validation, Writing – review & editing. **Wolfgang Knoll:** Conceptualization, Formal analysis, Funding acquisition, Resources, Supervision, Validation, Writing –

review & editing. **Fabio Biscarini:** Formal analysis, Funding acquisition, Resources, Supervision, Validation, Writing – review & editing. **Marcello Pinti:** Conceptualization, Funding acquisition, Project administration, Resources, Supervision, Validation, Writing – review & editing. **Carlo Augusto Bortolotti:** Conceptualization, Funding acquisition, Methodology, Project administration, Resources, Supervision, Validation, Writing – review & editing.

Declaration of competing interest

The authors declare that they have no known competing financial interests or personal relationships that could have appeared to influence the work reported in this paper.

Acknowledgments

This project has received funding from the European Union's Horizon 2020 research and innovation programme under the Marie Sklodowska-Curie grant agreement no. 813863. This project was supported by FISM - Fondazione Italiana Sclerosi Multipla - cod 2023/R-Single/016 and financed or co-financed with the "5 per mille" funding" to M.P. Furthermore, this work was supported by the Austrian Research Promotion Agency (FFG) within the COMET Project "PI-SENS" (Project No 915477) as well as by the Federal Provinces of Lower Austria and Tirol. This work was supported by the Gesellschaft für Forschungsförderung (GFF) of Lower Austria as part of the project "Aptamers and Odorant Binding Proteins – Innovative Receptors for Electronic Small Ligand Sensing'' (Project FTI22-G-012). J.D. acknowledges support from Operational Programme Johannes Amos Comenius financed by European Structural and Investment Funds and the Czech Ministry of Education, Youth and Sports (Project No. SENDISO -CZ.02.01.01/00/22_008/0004596). The research leading to these results has received funding from the European Union – NextGenerationEU through the Italian Ministry of University and Research under PNRR – M4C2-I1.3 Project PE_00000019 "HEAL ITALIA" (CUP E93C22001860006) to C.A. B. and M.B.

Appendix A. Supplementary data

Supplementary data to this article can be found online at https://doi.org/10.1016/j.biosx.2026.100826.

Data availability

The authors declare that the data supporting the findings of this study are available within the article and the supplemental information. The raw data supporting the present study are available on the repository Zenodo: 10.5281/zenodo.19224701.

References

Abouali, M., Rondelli, F., Genitoni, M., Murgia, M., Di Lauro, M., Fadiga, L., Biscarini, F., 2025. Electrodeposited reduced graphene oxide enables long-term memory in neuromorphic ambipolar electrolyte-gated transistors. Small 21, 2502768. https://doi.org/10.1002/smll.202502768.

Aspermair, P., Ramach, U., Reiner-Rozman, C., Fossati, S., Lechner, B., Moya, S.E., Azzaroni, O., Dostalek, J., Szunerits, S., Knoll, W., Bintinger, J., 2020. Dual monitoring of surface reactions in real time by combined surface-plasmon resonance and field-effect transistor interrogation. J. Am. Chem. Soc. 142, 11709–11716. https://doi.org/10.1021/jacs.9b11835.

Bellani, S., Fazzi, D., Bruno, P., Giussani, E., Canesi, E.V., Lanzani, G., Antognazza, M.R., 2014. Reversible P3HT/oxygen charge transfer complex identification in thin films exposed to direct contact with water. J. Phys. Chem. C 118, 6291–6299. https://doi.org/10.1021/jp4119309.

Berto, M., Casalini, S., Lauro, M.D., Marasso, S.L., Cocuzza, M., Perrone, D., Pinti, M., Cossarizza, A., Pirri, C.F., Simon, D.T., Berggren, M., Zerbetto, F., Bortolotti, C.A., Biscarini, F., 2016. Biorecognition in organic field effect transistors biosensors: the role of the density of states of the organic semiconductor. Anal. Chem. 88, 12330–12338. https://doi.org/10.1021/acs.analchem.6b03522.

Bhalla, N., 2026. Conundrums of localized surface Plasmon resonance biosensors. Small 22, e13520. https://doi.org/10.1002/smll.202513520.

Blasi, D., Sarcina, L., Tricase, A., Stefanachi, A., Leonetti, F., Alberga, D., Mangiatordi, G. F., Manoli, K., Scamarcio, G., Picca, R.A., Torsi, L., 2020. Enhancing the sensitivity of biotinylated surfaces by tailoring the design of the mixed self-assembled monolayer synthesis. ACS Omega 5, 16762–16771. https://doi.org/10.1021/acsomega.0c01717.

Cendra, C., Giovannitti, A., Savva, A., Venkatraman, V., McCulloch, I., Salleo, A., Inal, S., Rivnay, J., 2019. Role of the anion on the transport and structure of organic mixed conductors. Adv. Funct. Mater. 29. https://doi.org/10.1002/adfm.201807034.

Chennit, K., Delavari, N., Mekhmoukhen, S., Boukraa, R., Fillaud, L., Zrig, S., Battaglini, N., Piro, B., Noël, V., Zozoulenko, I., Mattana, G., 2023. Inkjet-printed, coplanar electrolyte-gated organic field-effect transistors on flexible substrates: fabrication, modeling, and applications in biodetection. Adv. Mater. Technol. 8. https://doi.org/10.1002/admt.202200300.

Coutinho, D.J., Feitosa, B. de A., Barbosa, H.F. de P., Colucci, R., Torres, B.B.M., Faria, G. C., 2023. Distinctive behavior of field-effect and redox electrolyte-gated organic transistors. J. Phys. Chem. C 127, 24443–24451. https://doi.org/10.1021/acs.jpcc.3c06261.

Dai, Shilei, Zhao, Yiwei, Wang, Yan, Zhang, Junyao, Fang, Lu, Jin, Shu, Shao, Yinlin, Huang, Jia, Dai, S., Zhao, Y., Wang, Y., Zhang, J., Fang, L., Huang, J., Jin, S., Shao, Y., 2019. Recent advances in transistor-based artificial synapses. Adv. Funct. Mater. 29, 1903700. https://doi.org/10.1002/ADFM.201903700.

De Salvo, A., Rondelli, F., Di Lauro, M., Tomassini, A., Greco, P., Stieglitz, T., Fadiga, L., Biscarini, F., 2023. Organic electronics circuitry for in situ real-time processing of electrophysiological signals. Adv. Mater. Interfac. 10, 2300583. https://doi.org/10.1002/admi.202300583.

Diacci, C., Berto, M., Di Lauro, M., Bianchini, E., Pinti, M., Simon, D.T., Biscarini, F., Bortolotti, C.A., 2017. Label-free detection of interleukin-6 using electrolyte gated organic field effect transistors. Biointerphases 12, 05F401. https://doi.org/10.1116/1.4997760.

Dundas, C.M., Demonte, D., Park, S., 2013. Streptavidin–biotin technology: improvements and innovations in chemical and biological applications. Appl. Microbiol. Biotechnol. 97, 9343–9353. https://doi.org/10.1007/s00253-013-5232-z.

Flagg, L.Q., Giridharagopal, R., Guo, J., Ginger, D.S., 2018. Anion-dependent doping and charge transport in organic electrochemical transistors. Chem. Mater. 30, 5380–5389. https://doi.org/10.1021/acs.chemmater.8b02220.

Gao, N., Zhou, W., Jiang, X., Hong, G., Fu, T.-M., Lieber, C.M., 2015. General strategy for biodetection in high ionic strength solutions using transistor-based Nanoelectronic sensors. Nano Lett. 15, 2143–2148. https://doi.org/10.1021/acs.nanolett.5b00133.

Giridharagopal, R., Guo, J., Kong, J., Ginger, D.S., 2021. Nanowire architectures improve ion uptake kinetics in conjugated polymer electrochemical transistors. ACS Appl. Mater. Interfaces 13, 34616–34624. https://doi.org/10.1021/acsami.1c08176.

Hageneder, S., Bauch, M., Dostalek, J., 2016. Plasmonically amplified bioassay – total internal reflection fluorescence vs. epifluorescence geometry. Talanta 156–157, 225–231. https://doi.org/10.1016/j.talanta.2016.05.023.

Hasler, R., Reiner-Rozman, C., Fossati, S., Aspermair, P., Dostalek, J., Lee, S., Ibáñez, M., Bintinger, J., Knoll, W., 2022. Field-effect transistor with a plasmonic fiber optic gate electrode as a multivariable biosensor device. ACS Sens. 7, 504–512. https://doi.org/10.1021/acssensors.1c02313.

Haustein, N., Gutiérrez-Sanz, Ó., Tarasov, A., 2019. Analytical model to describe the effect of polyethylene glycol on ionic screening of analyte charges in transistor-based immunosensing. ACS Sens. 4, 874–882. https://doi.org/10.1021/acssensors.8b01515.

Hojjat Jodaylami, M., Masson, J.-F., Badia, A., 2025. Surface plasmon resonance sensing. Nat. Rev. Methods Primers 5, 47. https://doi.org/10.1038/s43586-025-00417-8.

Homola, J., 2008. Surface plasmon resonance sensors for detection of chemical and biological species. Chem. Rev. 108, 462–493. https://doi.org/10.1021/cr068107d.

Homola, J., Yee, S.S., Gauglitz, G., 1999. Surface plasmon resonance sensors: review. Sens. Actuators B Chem. 54, 3–15. https://doi.org/10.1016/S0925-4005(98)00321-9.

Kotlarek, D., Curti, F., Vorobii, M., Corradini, R., Careri, M., Knoll, W., Rodriguez-Emmenegger, C., Dostálek, J., 2020. Surface plasmon resonance-based aptasensor for direct monitoring of thrombin in a minimally processed human blood. Sens. Actuators B Chem. 320, 128380. https://doi.org/10.1016/j.snb.2020.128380.

Kretschmann, E., Raether, H., 1968. Radiative decay of non radiative surface plasmons excited by light. Z. Für Naturforschung A 23, 2135–2136. https://doi.org/10.1515/zna-1968-1247.

Kyndiah, A., Zemignani, G.Z., Ronchi, C., Tullii, G., Khudiakov, A., Iachetta, G., Chiodini, S., Moreddu, R., Viola, F.A., Schwartz, P.J., Gomila, G., De Angelis, F., Sala, L., Antognazza, M.R., Caironi, M., 2025. Non-invasive action potential recordings using printed electrolyte-gated polymer field-effect transistors. Nat. Commun. 16, 8143. https://doi.org/10.1038/s41467-025-63484-1.

Li, J., Zhao, Y., Tan, H.S., Guo, Y., Di, C.A., Yu, G., Liu, Y., Lin, M., Lim, S.H., Zhou, Y., Su, H., Ong, B.S., 2012. A stable solution-processed polymer semiconductor with record high-mobility for printed transistors. Sci. Rep. 2. https://doi.org/10.1038/srep00754.

Liebermann, T., Knoll, W., 2000. Surface-plasmon field-enhanced fluorescence spectroscopy. Colloids Surf. A Physicochem. Eng. Asp. 171, 115–130. https://doi.org/10.1016/S0927-7757(99)00550-6.

Macchia, E., Manoli, K., Holzer, B., Franco, C.D., Ghittorelli, M., Torricelli, F., Alberga, D., Mangiatordi, G.F., Palazzo, G., Scamarcio, G., Torsi, L., 2018. Single-molecule detection with a millimetre-sized transistor. Nat. Commun. 9, 3223. https://doi.org/10.1038/s41467-018-05235-z.

Molazemhosseini, A., Viola, F.A., Berger, F.J., Zorn, N.F., Zaumseil, J., Caironi, M., 2021. A rapidly stabilizing water-gated field-effect transistor based on printed single-walled carbon nanotubes for biosensing applications. ACS Appl. Electron. Mater. 3, 3106–3113. https://doi.org/10.1021/acsaelm.1c00332.

Mor, D.C., Aktug, G., Schmidt, K., Asokan, P., Asai, N., Huang, C.-J., Dostalek, J., 2025. Plasmon-enhanced fluorescence (bio)sensors and other bioanalytical technologies. TrAC Trends Anal. Chem. 183, 118060. https://doi.org/10.1016/j.trac.2024.118060.

Mulla, M.Y., Tuccori, E., Magliulo, M., Lattanzi, G., Palazzo, G., Persaud, K., Torsi, L., 2015. Capacitance-modulated transistor detects odorant binding protein chiral interactions. Nat. Commun. 6, 6010. https://doi.org/10.1038/ncomms7010.

Nasi, M., Bianchini, E., De Biasi, S., Gibellini, L., Neroni, A., Mattioli, M., Pinti, M., Iannone, A., Mattioli, A.V., Simone, A.M., Ferraro, D., Vitetta, F., Sola, P., Cossarizza, A., 2020. Increased plasma levels of mitochondrial DNA and pro-inflammatory cytokines in patients with progressive multiple sclerosis. J. Neuroimmunol. 338, 577107. https://doi.org/10.1016/j.jneuroim.2019.577107.

Nguyen, T.T.K., Nguyen, T.N., Anquetin, G., Reisberg, S., Noël, V., Mattana, G., Touzeau, J., Barbault, F., Pham, M.C., Piro, B., 2018. Triggering the electrolyte-gated organic field-effect transistor output characteristics through gate functionalization using diazonium chemistry: application to biodetection of 2,4-dichlorophenoxyacetic acid. Biosens. Bioelectron. 113, 32–38. https://doi.org/10.1016/j.bios.2018.04.051.

Pallu, J., Avci-Adali, M., Mackeben, P., Mohammadnejad, L., Mattana, G., Noël, V., Piro, B., 2019. A DNA hydrogel gated organic field effect transistor. Org. Electron. 75, 105402. https://doi.org/10.1016/j.orgel.2019.105402.

Perlmann, G.E., Longsworth, L.G., 1948. The specific refractive increment of some purified proteins. J. Am. Chem. Soc. 70, 2719–2724. https://doi.org/10.1021/ja01188a027.

Picca, R.A., Manoli, K., Macchia, E., Sarcina, L., Franco, C.D., Cioffi, N., Blasi, D., Österbacka, R., Torricelli, F., Scamarcio, G., Torsi, L., 2020. Ultimately sensitive organic bioelectronic transistor sensors by materials and device structure design. Adv. Funct. Mater. 30. https://doi.org/10.1002/adfm.201904513.

Picca, R.A., Manoli, K., Macchia, E., Tricase, A., Franco, C.D., Scamarcio, G., Cioffi, N., Torsi, L., 2019. A study on the stability of water-gated organic field-effect-transistors based on a commercial p-Type polymer. Front. Chem. 7. https://doi.org/10.3389/fchem.2019.00667.

Porrazzo, R., Bellani, S., Luzio, A., Lanzarini, E., Caironi, M., Antognazza, M.R., 2014. Improving mobility and electrochemical stability of a water-gated polymer field-effect transistor. Org. Electron. 15, 2126–2134. https://doi.org/10.1016/j.orgel.2014.06.002.

Segantini, M., Ballesio, A., Palmara, G., Zaccagnini, P., Frascella, F., Garzone, G., Marasso, S.L., Cocuzza, M., Parmeggiani, M., 2022. Investigation and modeling of the electrical bias stress in electrolyte-gated organic transistors. Adv. Electron. Mater. 8. https://doi.org/10.1002/aelm.202101332.

Sensi, M., Oliveira, R.F. de, Berto, M., Palmieri, M., Ruini, E., Livio, P.A., Conti, A., Pinti, M., Salvarani, C., Cossarizza, A., Cabot, J.M., Ricart, J., Casalini, S., González-García, M.B., Fanjul-Bolado, P., Bortolotti, C.A., Samorì, P., Biscarini, F., 2023. Reduced graphene oxide electrolyte-gated transistor immunosensor with highly selective multiparametric detection of anti-drug antibodies. Adv. Mater. 35. https://doi.org/10.1002/adma.202211352.

Solodka, K., Berto, M., Ferraro, D., Menozzi, C., Borsari, M., Bortolotti, C.A., Biscarini, F., Pinti, M., 2022. Detection of neurofilament light chain with label-free electrolyte-gated organic field-effect transistors. Adv. Mater. Interfac. 9, 2102341. https://doi.org/10.1002/admi.202102341.

Spanu, A., Martines, L., Bonfiglio, A., 2021. Interfacing cells with organic transistors: a review of in vitro and in vivo applications. Lab Chip 21, 795–820. https://doi.org/10.1039/D0LC01007C.

Su, X., Wu, Y.-J., Robelek, R., Knoll, W., 2005. Surface plasmon resonance spectroscopy and quartz crystal microbalance study of Streptavidin film structure effects on biotinylated DNA assembly and target DNA hybridization. Langmuir 21, 348–353. https://doi.org/10.1021/la047997u.

Thomas, M.S., White, S.P., Dorfman, K.D., Frisbie, C.D., 2018. Interfacial charge contributions to chemical sensing by electrolyte-gated transistors with floating gates. J. Phys. Chem. Lett. 9, 1335–1339. https://doi.org/10.1021/acs.jpclett.8b00285.

Toma, M., Tawa, K., 2016. Polydopamine thin films as protein linker layer for sensitive detection of Interleukin-6 by surface plasmon enhanced fluorescence spectroscopy. ACS Appl. Mater. Interfaces 8, 22032–22038. https://doi.org/10.1021/acsami.6b06917.

Torricelli, F., Adrahtas, D.Z., Bao, Z., Berggren, M., Biscarini, F., Bonfiglio, A., Bortolotti, C.A., Frisbie, C.D., Macchia, E., Malliaras, G.G., McCulloch, I., Moser, M., Nguyen, T.-Q., Owens, R.M., Salleo, A., Spanu, A., Torsi, L., 2021. Electrolyte-gated transistors for enhanced performance bioelectronics. Nat. Rev. Methods Primers 1, 66. https://doi.org/10.1038/s43586-021-00065-8.

Tran, V.V., Jeong, G., Wi, E., Lee, D., Chang, M., 2023. Design and fabrication of ultrathin nanoporous donor–acceptor copolymer-based organic field-effect transistors for enhanced VOC sensing performance. ACS Appl. Mater. Interfaces 15, 21270–21283. https://doi.org/10.1021/acsami.3c00105.

Urbina, P.A.M., Berto, M., Greco, P., Sensi, M., Borghi, S., Borsari, M., Bortolotti, C.A., Biscarini, F., 2021. Physical insights from the Frumkin isotherm applied to electrolyte gated organic transistors as protein biosensors. J. Mater. Chem. C 9, 10965–10974. https://doi.org/10.1039/D1TC02546E.

Urbina, P.A.M., Paradisi, A., Hasler, R., Sensi, M., Berto, M., Saygin, G.D., Dostalek, J., Pinti, M., Greco, P., Borsari, M., Knoll, W., Bortolotti, C.A., Biscarini, F., 2024. Dynamic studies of antibody-antigen interactions with an electrolyte-gated organic transistor. Cell Rep. Phys. Sci. 5. https://doi.org/10.1016/j.xcrp.2024.101919.

Varhaug, K.N., Vedeler, C.A., Myhr, K.-M., Aarseth, J.H., Tzoulis, C., Bindoff, L.A., 2017. Increased levels of cell-free mitochondrial DNA in the cerebrospinal fluid of patients with multiple sclerosis. Mitochondrion 34, 32–35. https://doi.org/10.1016/j.mito.2016.12.003.

Wang, D., Noël, V., Piro, B., 2016. Electrolytic gated organic field-effect transistors for application in biosensors—A review. Electronics 5, 9. https://doi.org/10.3390/electronics5010009.

Wu, X., Liu, Q., Surendran, A., Bottle, S.E., Sonar, P., Leong, W.L., 2021. Enhancing the electrochemical doping efficiency in diketopyrrolopyrrole-based polymer for organic electrochemical transistors. Adv. Electron. Mater. 7, 2000701. https://doi.org/10.1002/aelm.202000701.

Zanotti, R., Berto, M., Sensi, M., Paradisi, A., Veronese, E., Pasquato, L., Bortolotti, C.A., Metrangolo, P., Biscarini, F., 2025. Fluorophobic effect enables selective detection of PFAS in water with electrolyte-gated organic transistors. Adv. Funct. Mater., e08425

Zhang, S., Ding, P., Ruoko, T.-P., Wu, R., Stoeckel, M.-A., Massetti, M., Liu, T., Vagin, M., Meli, D., Kroon, R., Rivnay, J., Fabiano, S., 2023. Toward stable p-type thiophene-based organic electrochemical transistors. Adv. Funct. Mater. 33. https://doi.org/10.1002/adfm.202302249.

Zhang, Y., Yao, X., Cui, Y., 2023. A DPP-DTT field-effect transistor-based biosensor for detecting Interleukin-6. IEEE Sensors Letters 7, 1–4. https://doi.org/10.1109/LSENS.2022.3224950.

Zhang, Y., Zeng, Q., Shen, Y., Yang, L., Yu, F., 2020. Electrochemical stability investigations and drug toxicity tests of electrolyte-gated organic field-effect transistors. ACS Appl. Mater. Interfaces 12, 56216–56221. https://doi.org/10.1021/acsami.0c15024.

Zhao, Z., Tian, Z., Yan, F., 2023. Flexible organic electrochemical transistors for bioelectronics. Cell Rep. Phys. Sci. 4. https://doi.org/10.1016/j.xcrp.2023.101673.